

SYNTHESIS OF NANO-IRON SUPPORTED BY GRAPHENE OXIDE/KAOLIN FOR THE TREATMENT OF LEAD IONS CONTAMINATED WATER

C. YU^a, M. ZHOU^a, X. N. YU^{a,*}, J. C. SHAO^a, X. Q. CAI^b

^aCollege of Civil Engineering and Architecture, Wenzhou University, Wenzhou, 325035, China

^bCollege of Chemistry and Materials Engineering, Wenzhou University, Wenzhou, 325035, China

In this experiment, kaolin/graphene oxide supported by nanometer zero-valent iron (GO-K-nZVI) was prepared by liquid phase reduction method. The kaolinite, graphene oxide (GO), nano-iron supported by kaolin (K-nZVI), and GO-K-nZVI was applied to remove Pb²⁺ ions. The microstructure and chemical composition of kaolinite, GO, K-nZVI, and GO-K-nZVI were characterized by X-ray techniques (XRD), Fourier transform infrared spectroscopy (FTIR), and Lorentz-Transmission Electron Microscope (TEM). Nanometer iron was easy to reunite and oxidize in the preparation process. Experiments showed that the support of graphene oxide/kaolin could alleviate the problem of agglomeration and oxidation. The GO-K-nZVI showed the best removal efficiency in various experimental environments (with time, pH, concentration of lead ions, and temperature). Time experiments showed that the removal efficiency of lead ions was 99% in 24 hours by GO-K-nZVI, higher than that of K-nZVI, Kaolin, and GO (91%, 33%, and 50%). The experiment results indicated that the removal efficiency of the lead ions in GO-K-nZVI and K-nZVI increased with the temperature increase, while kaolin and GO increased firstly and then decreased with the temperature increase. Most of nanometer irons in the GO-K-nZVI materials were 25 to 57 nm, and the dispersity was better than that of kaolin (K-nZVI). The removal efficiency of lead ions (Pb²⁺) was higher than that of kaolin load nano-iron (K-nZVI). The same content of nanometer iron in GO-K-nZVI was more efficient than K-nZVI.

(Received December 4, 2018; Accepted March 12, 2019)

Keywords: Graphene oxide, Nanoscale zerovalent, Kaolin, Lead ions, Removal efficiency

1. Introduction

Lead is a soft and toxic, belongs to heavy metals. Lead ions can enter into the body and produce injuries through the water, food, breathing, skin contact, etc., and damage adult nervous system, digestive system, lead to children's growth retardation, loss of appetite, walking inconvenience, lack of concentration, mental retardation, and other issues [1, 2]. Pb²⁺ ions can well be removed from wastewater and soil such as chemical precipitation [3], chemical reduction [4], ion exchange [5], mem-brane separation [6, 7], mineral adsorption [8], and biosorption, and so on

* Corresponding author: xnyu@wzu.edu.cn

[9]. However, these methods also have the disadvantages of long-term processing and require a large amount of processing costs, and are only applicable to low-concentration Pb^{2+} ions removal. In order to solve this problem, nanometer iron has been studied in silica, activated carbon, starch, polymers, and other substances, they can remove heavy metals from soil and groundwater [10, 11]. Many researches concerning nZVI has been carried out to remove metal ions such as: Cr^{6+} [12], Pb^{2+} [13], As^{3+} [14], etc. In short time, nZVI can remove metal ions and the removal rate are ideal [15]. However, similar to many other nano-materials, this ultra-fine powder, with a particle size less than 100nm, has a strong tendency to agglomerate into larger particles and is easy to be oxidized which can reduce reactive activity [16-18].

In this study, graphene oxide (GO) and kaolin were used to modify nZVI. Kaolin has a double-layer structure is mainly composed of Si-O tetrahedron. The crystal formula of kaolinite is $2\text{SiO}_2 \cdot \text{Al}_2\text{O}_3 \cdot 2\text{H}_2\text{O}$, and its theoretical composition is 46.54% of SiO_2 , 39.5% of Al_2O_3 , and 13.96% of H_2O . Üzüüm et al. had a dispersive effect on nano-iron by introducing kaolin as a carrier. Kaolin has a large specific surface area, which leads to its large surface energy and adsorption capacity. Therefore, kaolin is often used as adsorbent and flocculent in the process of water treatment. The experimental results show that kaolin can be used to support and disperse nanometer iron through its geometrical effect, thus reducing the agglomeration of nanometer iron particles. At the same time, kaolin may have a certain adsorption capacity for pollutants, which can play a preconcentration role in the degradation of pollutants. The research results showed that the introduction of kaolin doesn't always lead to load type nanometer iron direct rights of specific surface area is large, but under the same conditions was applied to repair of pollutants, the effect of the latter is superior to the former, this strongly proves the carrier, to improve the activity of iron nanoparticles [20-22]. In this study, kaolin was used to support nanoscale iron (K-nZVI). Graphene oxide was added to the solution as additive for improving the removal efficiency of Pb^{2+} ions upon K-nZVI.

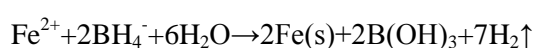
2. Materials and methods

2.1. Materials

Kaolin, Ferric chloride tetrahydrate, sodium borohydride, anhydrous ethanol, sodium hydroxide and lead nitrate were purchased from Sinopharm Chemical Reagent Co., Ltd. Graphene oxide (thickness: 0.55-1.2 nm, diam.: 0.5-3 μm , layers: <3, purity: 99%) was purchased from J&K Scientific LTD.

2.2 Preparation of graphene oxide/kaolin supported nanometer iron (GO-K-nZVI)

Graphene oxide (0.3g) and high purity water (200ml) were mixed by ultrasonic vibration for 30 min in a beaker. 1.8g of kaolin was added to above solution and stirring 2 h. 4.275g of Ferric chloride tetrahydrate was added into the mixed solution of kaolin and graphene oxide for stirring 1 h. Then, 200 mL of absolute ethanol mixed with the above mixed solution by ultrasonic vibration 1 h after stirring 1 h. Sodium borohydride (9.768g, 50mL, pH=11) was slowly added to the above mixed solution and stirring 20 min. Finally, the specimen was kept in -85°C , named as GO-K-nZVI. K-nZVI, the reaction formula was as following [12, 16]:



2.3. Characterization of materials

Specific surface area was tested by the BET-N₂ (Micromeritics ASAP2020HD88 Chemisorption Surface Area Analyzer, Micromeritics instrument (Shanghai) Ltd.). X-ray techniques (XRD, Bruker Company, Germany) analysis of samples was carried by D8-Advance X diffraction meter (40kv, 40mA) with Cu ($\lambda=1.5406\text{\AA}$). Fourier transform infrared spectroscopy (FTIR) of samples was determined by TENSOR27 FTIR (Zhengzhou Great Wall Science and Industry Co., Ltd., 4000-400cm⁻¹). Scanning Electron Microscopy (SEM) images of specimens were tested by JSM-6700F. Lorentz-Transmission Electron Microscope (TEM) images of the specimens were observed via JEM, 2100F equipment.

2.4. Removal efficiency of lead ions

Different concentration of lead ions was prepared by dissolving certain mass of lead nitrate in high purity water. We used the Atomic Absorption Spectrometer (Shimadzu technology trading company) to determine the concentration of Pb²⁺ ions before and after adsorption. The adsorbent dose of 1 g/L (kaolin, K-nZVI, GO-K-nZVI and GO) was in Pb²⁺ ions contaminated water, then vibrated for 5 minutes with ultrasonic wave, and the solution was placed in a constant temperature and humidity laboratory. The removal efficiency of lead ions is calculated by the following formula [16]:

$$R=(1-\frac{c_e}{c_o})*100\%$$

where R represents the removal efficiency of lead ions (%), C_o is the initial concentration of lead ions (mg/L), and C_e represents the concentration of Pb²⁺ ions after t time (mg/L).

3. Results and discussion

3.1. Composition and microstructure of kaolin, K-nZVI, GO-K-nZVI, and GO

As can be seen from Fig. 1a, there were two strong absorption peaks in kaolin at 3696 cm⁻¹ and 3623cm⁻¹, and the absorption band in the range of 3700cm⁻¹ ~ 3600cm⁻¹ was caused by the stretching vibration of hydroxyl (OH) in kaolin [16]. It is generally believed that the absorption band near 3620cm⁻¹ was caused by the internal OH, and the absorption band near 3700cm⁻¹ was caused by the inner surface OH [16]. There was a strong absorption band at 1634 cm⁻¹ in the middle and low frequency region, which was the absorption band of the asymmetric stretching vibration of Si-O-Si and the telescopic vibration of O-Si-O. The Si-O stretching vibration was mainly between 1120cm⁻¹ ~ 1000cm⁻¹ [16]. In addition, the band of 1038 cm⁻¹ represented the stretching of Si-O of tetrahedron [16, 23]. The bending vibration of OH was mainly between 950cm⁻¹ ~ 780cm⁻¹. Silicon dioxide, aluminum oxide, and water was existed in the kaolin. Compared with kaolin, K-nZVI had the similar absorption peak. It can be found that kaolin was not destroyed and a dispersed role. Figure 1b showed FTIR spectrum of GO and GO-K-nZVI. The peaks at 1227cm⁻¹, 1626cm⁻¹, 1730cm⁻¹ was stretching vibration of C-O-C, C=C, and C=O, respectively [16, 24]. The peak at 1051cm⁻¹ was the stretching vibration of C-O-C, 3428 cm⁻¹ was OH [16, 25]. The GO structure was not damaged [16].

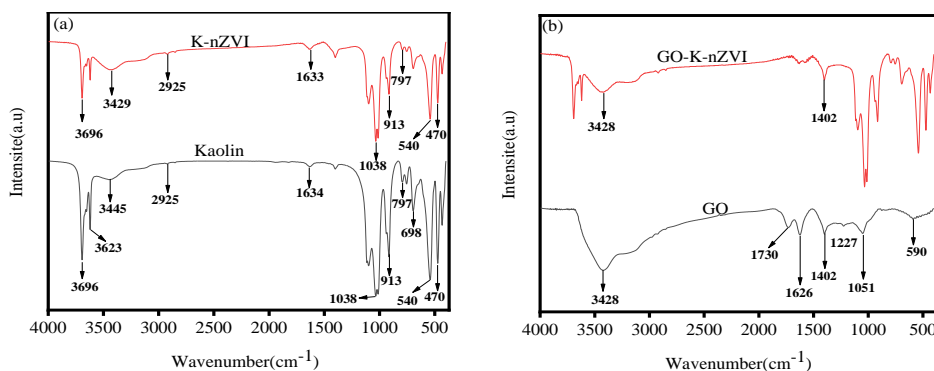


Fig. 1. FTIR spectra of synthetic materials.

The XRD patterns showed kaolin, K-nZVI, GO-K-nZVI, and GO, as shown in Fig. 2. The characteristic diffraction peak of iron was 44.75° , corresponding to zero-valent iron (α -Fe) [16]. It was also confirmed in the newly prepared K-nZVI and had been described in relevant study [26]. It means that nZVI existed in the K-nZVI and GO-K-nZVI prepared by 2.2 method. The results indicated that zero-valent iron was successful and feasible in the experiment.

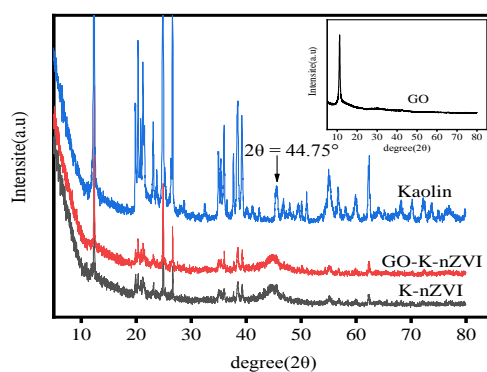


Fig. 2. XRD patterns of kaolin, K- nZVI, GO-K-nZVI, and GO.

The BET area of kaolin, K-nZVI, GO-K-nZVI, and GO was shown in Table 1[16]. The BET area of K-nZVI was $25.03 \text{ m}^2\text{g}^{-1}$, which was larger than that of Kaolin ($9.18 \text{ m}^2\text{g}^{-1}$). Kaolin could reduce the agglomeration of nZVI. The mean pore diameter of kaolin was 12.37 nm which was smaller than that of K-nZVI (13.1 nm), indicating that nZVI could expand the kaolin layer clearance. The BET area of GO-K-nZVI was $34.73 \text{ m}^2\text{g}^{-1}$, indicating that GO could enlarge the specific surface area of K-nZVI [16]. The addition of GO could improve dispersed state of nZVI and modify nZVI.

Table1. The BET area of the samples.

samples	Surface area (m^2/g)	Mean pore diameter (nm)
Kaolin	9.18	12.37
GO	53.80	18.75
K-nZVI	25.03	13.10
GO-K-nZVI	34.73	25.38

The morphology of four different materials could be seen in Figure 3. To prevent the aggregation of nZVI, Kaolin provided a good platform structure for nZVI, as shown in Fig. 3(b). It can be seen from Fig. 3(c) that iron particles were dispersed in kaolin and attached to the surface of kaolin. These phenomena could also be seen in other study [27]. In Fig. 3 (a), GO had a large specific surface area and could disperse iron particles to a certain extent. In Fig. 3(d), kaolin and graphene oxide modified iron particles were spherical, evenly distributed on the surface of kaolin and graphene oxide.

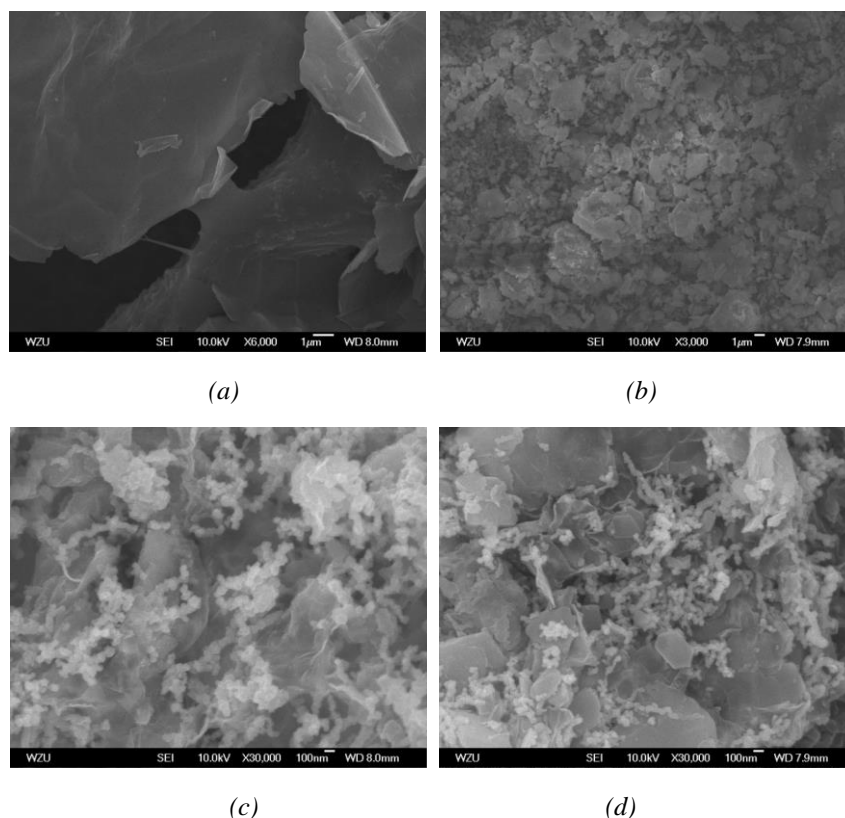


Fig. 3. SEM images of (a) GO, (b) Kaolin, (c) K-nZVI, and (d) GO-K-nZVI.

The TEM images of the samples (Kaolin, GO, K-nZVI, GO-K-nZVI) were shown in Fig. 4. Kaolin and GO showed flake structure, which provided a good platform for the loading of iron particles [16]. Fig. 4(c) showed the TEM image of K-nZVI. The nZVI formation chain on the surface of kaolin, and the particle size of nZVI was nanoscale. Fig. 4(d) showed the TEM image of GO-K-nZVI, the nZVI was more dispersed, with diameters ranging from 24.55 nm to 57.10 nm and mean value of 37.84 nm. Table 2 showed the diameter distribution of nZVI in K-nZVI and GO-K-nZVI in particle size bar charts, respectively. From TEM and SEM, nZVI of GO-K-nZVI was more evenly distributed than that of K-nZVI, reduced agglomeration of iron particles and chain-like iron particles and increased the dispersion of iron particles.

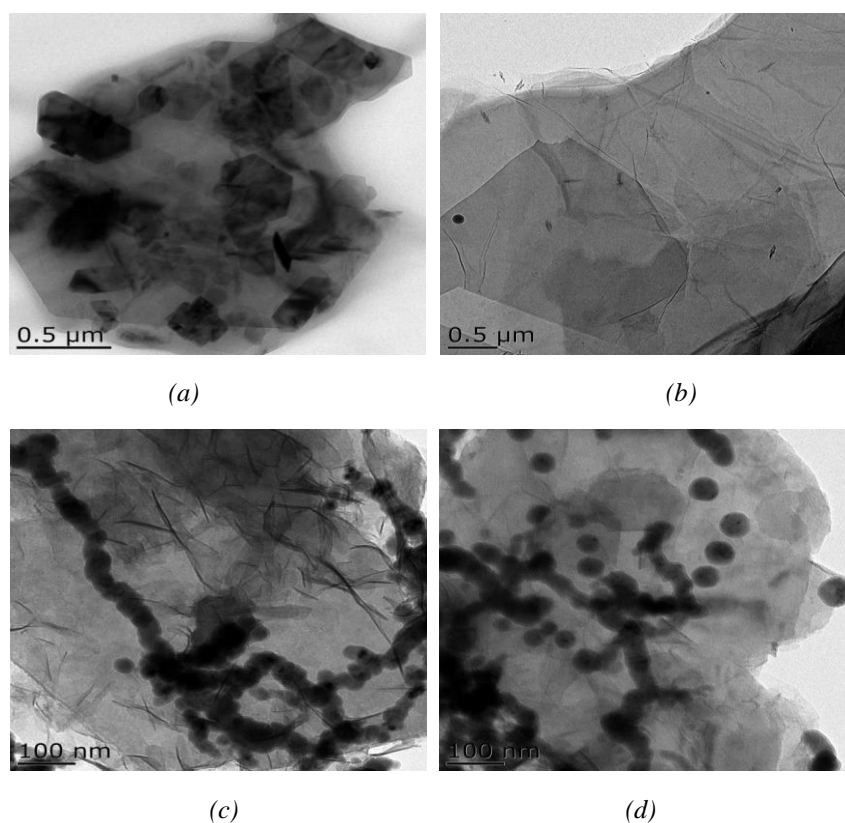
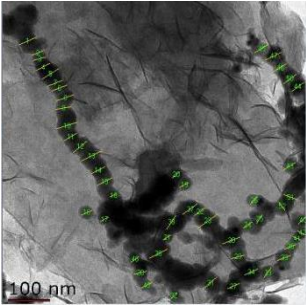
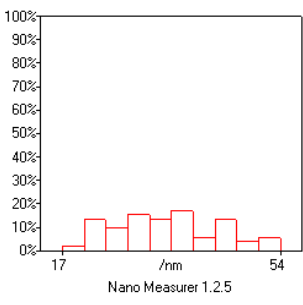
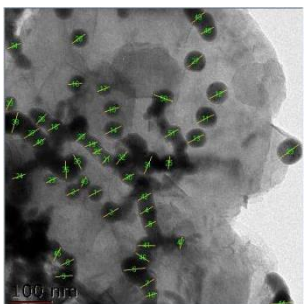
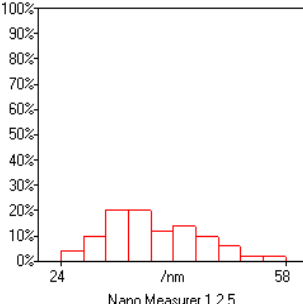


Fig. 4. TEM images of (a) Kaolin, (b) GO, (c) K-nZVI, and (d) GO-K-nZVI.

Table 2. The diameter distribution of nZVI in K-nZVI and GO-K-nZVI.

samples	Particle size diagram of iron particles under TEM.	Particle size bar chart.	The value of the particle size (nm)
K-nZVI			The biggest size: 53.33 The minimum size: 17.65 The average particle size: 34.90
GO-K-nVI			The biggest size: 57.10 The minimum size: 24.55 The average particle size: 37.84

3.2 The effect of time, concentration, pH, and temperature of on removal efficiency of lead ions

Fig. 4 showed the removal effect of GO-K-nZVI, K-nZVI, GO, and kaolin within 24h. The lead ions of removal rate by GO-K-nZVI were better than that of kaolin, K-nZVI, and GO. When pH was 5 ± 0.3 , adsorbent was 1g/L, concentration of lead ions was 200mg/L, temperature was 18°C, the removal rate of GO-K-nZVI and K-nZVI reached 99% and 91% after 24 h, respectively. Removal rate of lead ions by GO and kaolin were 50% and 33%, respectively. The removal rate of lead ions in four different substances for 16 h was relatively fast and tended to be gentle between 16 h and 24 h. The removal rate of lead ions via kaolin was minimum than GO-K-nZVI, K-nZVI, and GO.

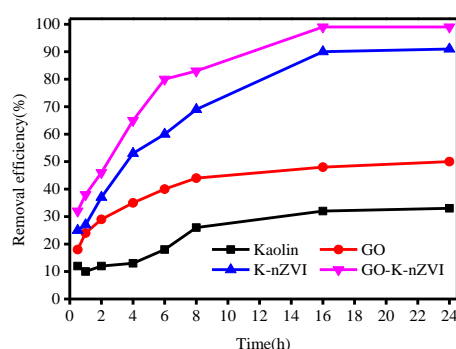


Fig. 4. Removal efficiency of lead ions by GO-K-nZVI, K-nZVI, GO, and kaolin with time.

Fig. 5 showed the effect of different lead ions concentrations on the removal rate of lead ion in GO-K-nZVI, K-nZVI, GO and kaolin. The concentration of lead ions was 100, 150, 200, 250, 300, 350 and 400mg/L. 0.1g of GO-K-nZVI was added to different concentration of lead ions (100mL). The removal time, pH and temperature are 24h, 5 ± 0.3 and 18°C, respectively. With the increase of initial concentration, the removal efficiency of different adsorbents decreased from Figure 5. When the initial concentration of Pb^{2+} ions was 150 mg/L, removal efficiency of Pb^{2+} ions can reach 99% and 97% by GO-K-nZVI and K-nZVI, respectively. However, the initial concentration of Pb^{2+} ions was 400 mg/L, removal efficiency of the GO-K-nZVI and K-nZVI was 75% and 63%, respectively. This is because the concentration of lead ions was too high and the adsorption capacity of iron particles was limited. The iron particles reached adsorption saturation before the high concentration of lead ions was absorbed completely [28, 29]. The removal rate of lead ions by GO-K-nZVI and K-nZVI had the better effect than GO and kaolin. The GO-K-nZVI was better than K-nZVI, and it had the best removal effect.

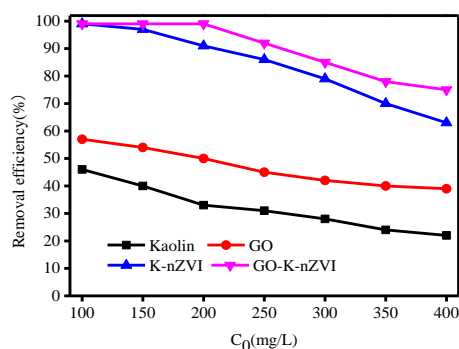


Fig. 5. Removal efficiency of lead ions by GO-K-nZVI, K-nZVI, GO, and kaolin with concentration of lead ions.

Obviously, the pH of solution is an important parameter affecting the adsorption performance. At a certain pH, when the adsorbent was 1 g/L, the removal rate of lead ions increases with the increase of pH. The concentration of lead ions was 200 mg/L. The temperature was 18. The time was 8 h. As can be seen from Figure 6, pH had a great influence on the adsorption of Pb^{2+} ions. As pH gradually increased from 3 to 7, the adsorption amount also increased. In an acidic environment (pH=3), GO-K-nZVI, K-nZVI, GO, and kaolin had lower lead ions of removal rate. Lead ions removal rate of the kaolin was only 7%, which was the smallest, under the condition of low pH, Pb^{2+} ions removal effect was a bit poor, this may be due to the high quality of H^+ concentration in the solution at this time, hold on the adsorbent adsorption, and the competitive adsorption of heavy metal ions, thus inhibiting the adsorbent for heavy metal ions adsorption [30-32]. When the pH = 7, GO-K-nZVI lead ions of removal rate reached 90%, higher than that of K-nZVI (79%), GO (63%), kaolin (42%). Therefore, increasing graphene oxide can improve the removal rate of lead ions.

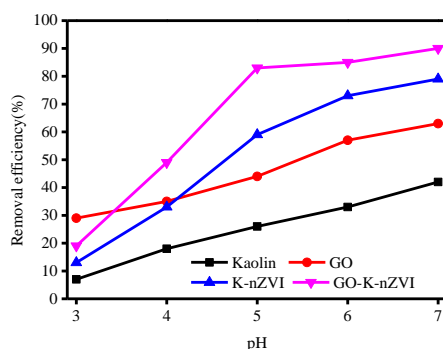


Fig. 6. Removal efficiency of lead ions by GO-K-nZVI, K-nZVI, GO, and kaolin with pH.

The effect of temperature on the removal efficiency of lead ions was shown in Fig. 7. Under a certain range of temperature, when adsorbent is 1g/L and concentration of lead ions was 200mg/L, time was 4h, the removal rate of lead ions by GO-K-nZVI and K-nZVI increased with the increase of temperature. The increase of temperature led to the obvious increase of the removal rate of lead ions by K-nZVI and GO-K-nZVI. For Kaolin, the influence of temperature on the removal rate of lead ions was not obvious. For GO, the removal rate of lead ions slowly increased

with the rise of temperature (20°C ~ 50°C), and then slowed down between 50°C to 60°C. We can see that the removal rate of lead ions by GO-K-nZVI and K-nZVI had the better effect than GO and kaolin. Therefore, GO-K-nZVI was better than K-nZVI, and it had the best removal effect.

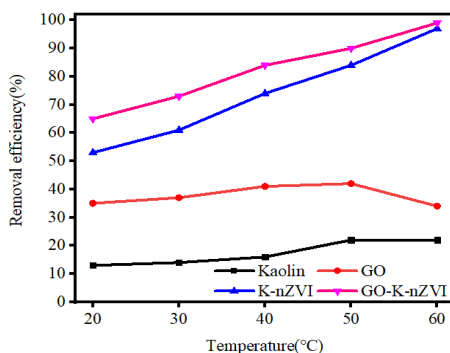


Fig. 7. Removal efficiency of lead ions by GO-K-nZVI, K-nZVI, GO, and kaolin with temperature.

4. Conclusions

In the study, graphene oxide/kaolin supported nano-iron was prepared by liquid phase reduction technique, which solved the problem of easy oxidation and condensation of nano-iron. The kaolin/graphene oxide (GO-K-nZVI) can well remove lead ions in aqueous solution. Obviously, nZVI aggregation can be eliminated, and nZVI successfully adheres to kaolin and graphene oxide surfaces. As an effective dispersant and stabilizer, kaolin could reduce aggregation, increased specific surface area and improved reactivity in the composite support system. Experiments showed that the K-nZVI composition is better than kaolin when Pb^{2+} ions were removed from aqueous solution. However, the GO-K-nZVI composition was better than K-nZVI. K-nZVI and GO-K-nZVI were highly efficient and promising active materials, and further studies will be needed in the future.

Acknowledgments

This work was supported by the National Nature Science Foundation of China (Grant No. 51702238, 51578427, 51572197, and 41372264), the Plan Project of Science and Technology of Zhejiang Province (No. 2014C33015 and 2015C33220), Opening Funds of Jiangsu Key Laboratory of Construction Materials (No. CM2018-02), and the Plan Project of Science and Technology of Wenzhou (No. ZS2017002).

References

- [1] Y. H. Li, Z. H. Di, J. Ding, D. H. Wu, Z. K. Luanc, Y. Q. Zhua, *Water Res.* **39**, 605 (2005).
- [2] B. B. Gump, M. J. Dykas, J. A. MacKenzie, A. K. Dumas, B. Hruska, C. K. Ewart, P. J. Parsons, C. D. Palmer, K. Bendinskas, *Environ. Res.* **158**, 576 (2017).

- [3] O. X. Leupin, S. J. Hug, A. B. M. Badruzzaman, *Environ. Sci. Technol.* **39**, 8032 (2005).
- [4] S. M. Ponder, J. G. Darab, T. E. Mallouk, *Environ. Sci. Technol.* **34**, 2564 (2000).
- [5] M. S. Berber-Mendoza, R. Leyva-Ramos, P. Alonso-Davila, L. Fuentes-Rubio, R. M. Guerrero-Coronado, *J. Colloid Interface Sci.* **301**, 40 (2006).
- [6] Y. M. Sang, F. S. Li, Q. B. Gu, C. Z. Liang, J. Q. Chen, *Desalination* **223**, 349 (2008).
- [7] S. Mohtada, M. Toraj, I. Javad, K. Norollah, *Chem. Eng. J.* **144**, 431 (2008).
- [8] Y. G. Chen, Y. He, W. M. Ye, L. Y. Jia, *China. J. Ind. Eng. Chem.* **26**, 335 (2015).
- [9] Y. G. Chen, Y. He, W. M. Ye, C. H. Lin, X. F. Zhang, B. Ye, *Environ. Earth Sci.* **67**, 1261 (2012).
- [10] P. Huang, Z. Ye, W. Xie, Q. Chen, J. Li, Z. Xu, M. Yao, *Water Res.* **47**, 4050 (2013).
- [11] X. Zhao, W. Liu, Z. Cai, B. Han, T. Qian, D. Zhao, *Water Res.* **100**, 245 (2016).
- [12] J. Shang, M. Zong, Y. Yu, X. Kong, Q. Du, Q. Liao, *J. Environ. Manag.* **197**, 331 (2017).
- [13] Q. Y. Liu, Y. L. Bei, Z. Feng, *Cent. Eur. J. Chem.* **7**, 79 (2009).
- [14] T. Liu, Y. Yang, Z. L. Wang, Y. Sun, *Chem. Eng. J.* **288**, 739 (2016).
- [15] H. Su, Z. Fang, P. E. Tsang, L. Zheng, W. Cheng, J. Fang, D. Zhao, *J. Hazard. Mater.* **318**, 533 (2016).
- [16] J. C. Shao, X. N. Yu, M. Zhou, X. Q. Cai, C. Yu, *Materials* **11**, 945 (2018).
- [17] Y. Sun, C. Lei, E. Khan, S. S. Chen, D. C. Tsang, Y. S. Ok, D. Lin, Y. Feng, X. D. Li, *Chemosphere* **176**, 315 (2017).
- [18] H. K. Boparai, M. Joseph, D. M. O'Carroll, *J. Hazard. Mater.* **1986**, 458 (2011).
- [19] N. Arancibia-Miranda, S. E. Baltazar, A. García, A. H. Romero, M. A. Rubio, D. Altbir, *Mater. Res. Bull.* **59**, 341 (2014).
- [20] X. Zhang, S. Lin, X. Q. Lu, Z. Chen, *Chem. Eng. J.* **163**, 243 (2010).
- [21] D. Li, M. B. Müller, S. Gilje, R. B. Kaner, G. G. Wallace, *Nat. Nanotechnol.* **3**, 101 (2008).
- [22] M. Terrones, A. R. Botello-Méndez, J. Campos-Delgado, F. López-Urías, Y. I. Vega-Cantú, F. J. Rodríguez-Macías, A. L. Elías, E. Muñoz-Sandoval, A. G. Cano-Márquez, J. Charlier, H. Terrones, *Nano Today* **5**, 351 (2010).
- [23] X. Jin, Z. Chen, R. Zhou, Z. Chen, *Mater. Res. Bull.* **61**, 433 (2015).
- [24] H. Raghubanshi, S. M. Ngoben, A. O. Osikoya, N. D. Shooto, C. W. Dikio, E. B. Naidoo, E. D. Dikio, R. K. Pandey, R. Prakash, *J. Ind. Eng. Chem.* **47**, 169 (2017).
- [25] Y. Shang, T. Li, Y. Yin, H. Li, A. Dang, L. Zhang, X. Chen, Y. Zhang, C. Xiong, T. Zhao, *J. Anal. Appl. Pyrol.* **120**, 215 (2016).
- [26] L. N. Shi, X. Zhang, Z. L. Chen, *Water Res.* **45**, 886 (2011).
- [27] Ç. Üzümlü, T. Shahwan, A. E. Eroğlu, K. R. Hallam, T. B. Scott, I. Lieberwirth, *Appl. Clay Sci.* **43**, 172 (2009).
- [28] J. T. Nurmi, P. G. Tratnyek, V. Sarathy, D. R. Bear, J. E. Amonette, K. Peacher, C. Wang, J. C. Linehan, D. W. Matson, R. L. Penn, M. D. Driessen, *Environ. Sci. Technol.* **39**, 1221 (2005).
- [29] X. Q. Li, W. X. Zhang, *J. Phys. Chem. C* **111**, 6939 (2007).
- [30] J. Li, Y. Li, Q. Meng, *J. Hazard. Mater.* **174**, 188 (2010).
- [31] J. Zhu, V. Cozzolino, M. Pigna, Q. Huang, A. G. Caporale, A. Violante, *Chemosphere* **84**, 484 (2011).
- [32] X. Zhang, Y. Lin, X. Shan, Z. Chen, *Chem. Eng. J.* **158**, 566 (2010).